Supplementary Materials for

Dynamic photomask directed lithography based on electrically stimulated nematic liquid crystal architectures

Mengjun Liu[1]†, Ruizhi Yang[3]†, Zhenghao Guo[3]†, Kexu Chen[3], Haoqiang Feng[3], Han Lu[1], Shijian Huang[1], Minmin Zhang[1], Huapeng Ye[3]*, Lingling Shui[1, 2, 3]*

[1]Guangdong Provincial Key Laboratory of Nanophotonic Functional Materials and Devices, School of Information and Optoelectronic Science and Engineering, South China Normal University, Guangzhou 510006, China.

[2]Guangdong Basic Research Center of Excellence for Structure and Fundamental Interactions of Matter, South China Normal University, Guangzhou 510006, China.

[3]Joint Laboratory of Optofluidic Technology and Systems, National Center for International Research on Green Optoelectronics, South China Academy of Advanced Optoelectronics, South China Normal University, Guangzhou 510006, China.

*Corresponding authors: Huapeng Ye (yehp@m.scnu.edu.cn)

Lingling Shui (shuill@m.scnu.edu.cn)

This PDF file includes:

Supplementary Text

Supplementary Figs. 1 to 8

Other Supplementary Materials for this manuscript include the following:

Movies S1 to S2

Supplementary Text

Computational model

The Landau-de Gennes's *Q* tensor is employed to represent the uniaxial LC, and the *Q* is defined as following:

$$\boldsymbol{Q} = S\left(\boldsymbol{n}\otimes\boldsymbol{n} - \frac{1}{3}\boldsymbol{I}\right) = S\begin{pmatrix} n_1n_1 - 1/3 & n_1n_2 & n_1n_3 \\ n_1n_2 & n_2n_2 - 1/3 & n_2n_3 \\ n_3n_1 & n_3n_2 & n_3n_3 - 1/3 \end{pmatrix} (S1)$$

where $\boldsymbol{I}$ is the identity matrix, S is the order parameter, Q_{ij} is used to denote the ij^{th} element of $\boldsymbol{Q}$. As $\boldsymbol{Q}$ is a symmetric traceless matrix, it has six different elements, namely Q_{11}, Q_{22}, Q_{33}, Q_{12}, Q_{13}, and Q_{23}.

The Q tensor (Eq. (1)) and the potential U to represent the elastic free energy density f_d and the electric free energy density f_e.

$$f_d = \sum_{\substack{i=1,2,3\\ j=1,2,3\\ k=1,2,3}} \left[\frac{L_1}{2}\left(\frac{\partial Q_{ij}}{\partial \xi_k}\right)^2 + \frac{L_2}{2}\frac{\partial Q_{ij}}{\partial \xi_j}\frac{\partial Q_{ik}}{\partial \xi_k} + \frac{L_3}{2}\frac{\partial Q_{ik}}{\partial \xi_j}\frac{\partial Q_{ij}}{\partial \xi_k} \right] + \sum_{\substack{i=1,2,3\\ j=1,2,3\\ k=1,2,3\\ l=1,2,3}} \left[\frac{L_4}{2} e_{lik} Q_{lj}\frac{\partial Q_{ij}}{\partial \xi_k} + \frac{L_6}{2} Q_{lk}\frac{\partial Q_{ij}}{\partial \xi_l}\frac{\partial Q_{ij}}{\partial \xi_k} \right] (S2)$$

where $(\xi_1, \xi_2, \xi_3) = (x, y, z)$ is the Cartesian coordinate system, and e_{lik} is the Levi-Civita symbol ($e_{xyz} = e_{yzx} = e_{zxy} = 1$, $e_{zyx} = e_{yxz} = e_{xzy} = -1$, and all other $e_{ijk} = 0$). The elastic parameters L_i are given as $L_1 = (k_{33}\text{-}k_{11}\text{+}3k_{22})/(6S^2)$, $L_2 = (k_{11}\text{-}k_{22}\text{-}k_{24})/S^2$, $L_3 = k_{24}/S^2$, $L_4 = 2q_0\,k_{22}/S^2$, $L_6 = (k_{33}\text{-}k_{11})/(2S^2)$, where $q_0 = 2\pi/p$, p is the helical pitch of cholesteric LC; k_{11}, k_{22}, k_{33}, and k_{24} are the corresponding splay, twist, bend, and saddle-splay elastic constant, respectively. The term k_{24} is negligible in most parallel LC cells.

The electric free energy density of the Q tensor is expressed as:

$$f_e = \sum_{\text{i=1,2,3}} \left[\varepsilon_0 \frac{2\varepsilon_\perp + \varepsilon_{/\!/}}{6}\frac{\partial U}{\partial \xi_i}\frac{\partial U}{\partial \xi_i} \right] + \sum_{\substack{\text{i=1,2,3}\\ j=1,2,3}} \left[\frac{Q_{ij}}{2S}\varepsilon_0\left(\varepsilon_{/\!/}\text{-}\varepsilon_\perp\right)\frac{\partial U}{\partial \xi_i}\frac{\partial U}{\partial \xi_{\text{j}}} \right] (S3)$$

where ε_0 is vacuum permittivity, $\varepsilon_\perp$ and $\varepsilon_{/\!/}$ are the vertical and horizontal permittivity of LC molecule respectively.

Hence, the total energy F_g can be obtained by integrating the Gibbs free energy density f_g over the volume, namely $F_g = \int f_g \, \mathrm{d}v = \int f_d - f_e \, \mathrm{d}v$.

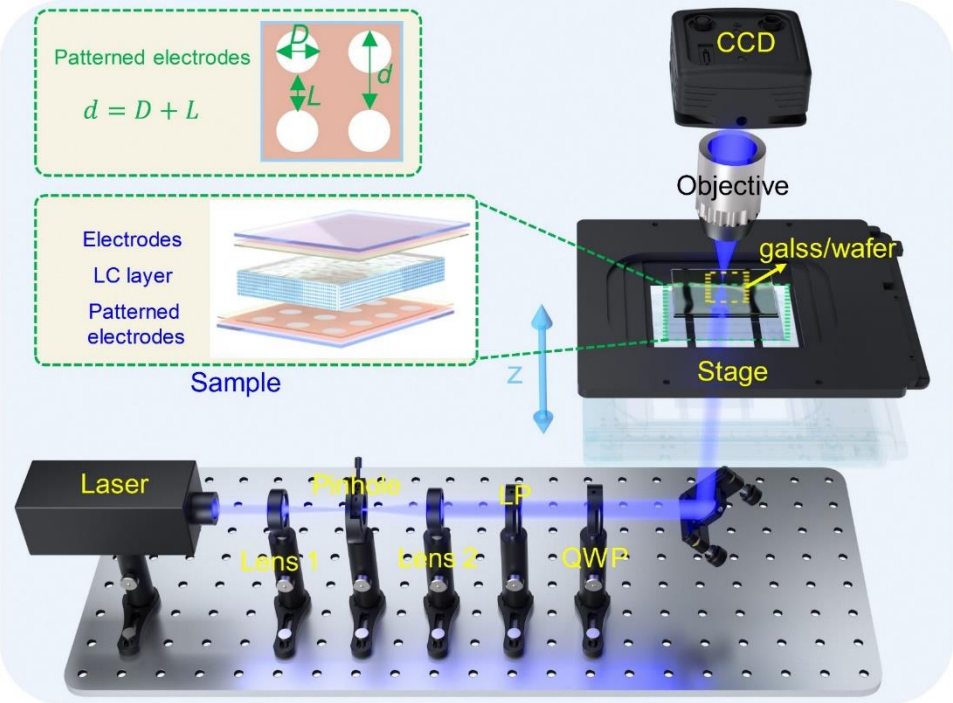

Supplementary Fig. 1.

Schematic diagram of the experimental setup.

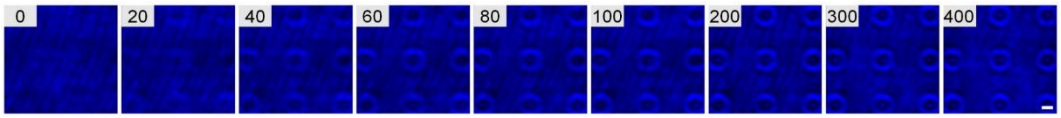

Supplementary Fig. 2.

Experimentally observed OM images of diffraction patterns respond to voltage (U = 0, 20, 40, 60, 80, 100, 200, 300, 400 Vpp). There is no discernible diffraction pattern in the OFF state (0 Vpp), whereas the diffraction pattern gradually becomes visible (40 Vpp), ultimately stabilizing when the voltage surpassed 80 Vpp. The experimental parameters are: D = 20.11, L = 19.89 μm, H = 50 μm, λ = 405 nm, and z = 300 μm. Scale bar: 10 μm.

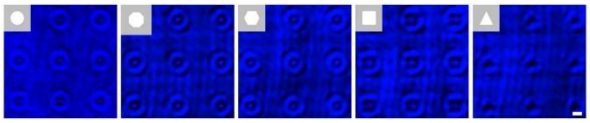

Supplementary Fig. 3.

Experimentally observed OM images of diffraction patterns use different electrode shapes for circular, octagonal, hexagonal, square, and triangular aperture arrays. For the circular aperture, the resultant diffraction pattern tends to be circularly shaped. In case of octagonal or hexagonal aperture with an electrode aperture size of 20 μm, the shapes of the diffraction pattern extremely resemble circle, although there are slight deviations due to the aperture shape. When the square aperture is used, a distinct diffraction pattern with four corners appears. On the other hand, the diffraction pattern for the triangular aperture exhibits a triangle shape, stemming from the enhanced distribution of electric field lines resulting from the reduced effective area of no ITO. Consequently, the degree of orientation for the NLC molecules along the direction of the applied electric field is weakened, leading to a simpler diffraction pattern. The experimental parameters are: D = 20.11 μm, L = 19.89 μm, H = 50 μm, U = 400 Vpp, λ = 405 nm, and z = 250 μm. Scale bar: 10 μm.

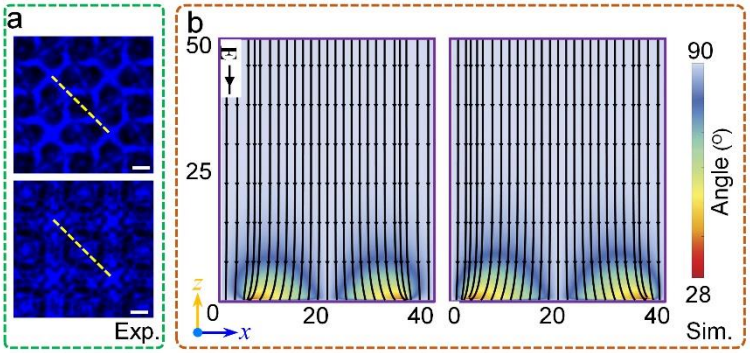

Supplementary Fig. 4.

(**a**) Experimentally observed OM images of R = 0.289, and (**b**) correspondingly calculated NLC molecular orientation of x-z plane aligning to the electric field lines (E) when D = 29.87, L = 10.13 μm, and D = 35.05, L = 5.95 μm, respectively. The experimental parameters are: H = 50 μm, U = 400 Vpp, and λ = 405 nm. Scale bar: 10 μm.

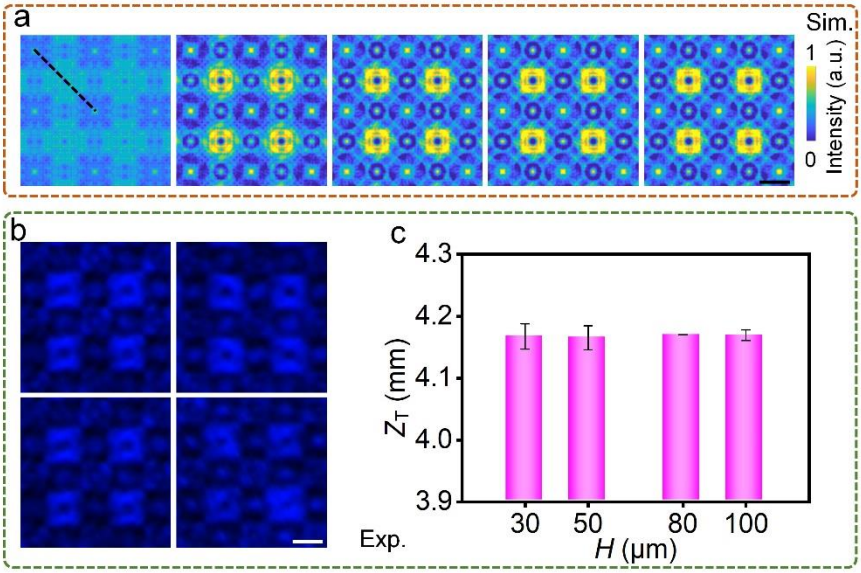

Supplementary Fig. 5.

(**a**) Simulated diffraction patterns with H = 1, 5, 9, 30, 50 μm. (**b**) Experimentally observed OM images and (**c**) Z_T values when H = 30, 50, 80, 100 μm. The experimental parameters are: D = 20.11 μm, L = 19.89 μm, R = 0.56, U = 400 Vpp, and λ = 405 nm. Scale bar: 20 μm.

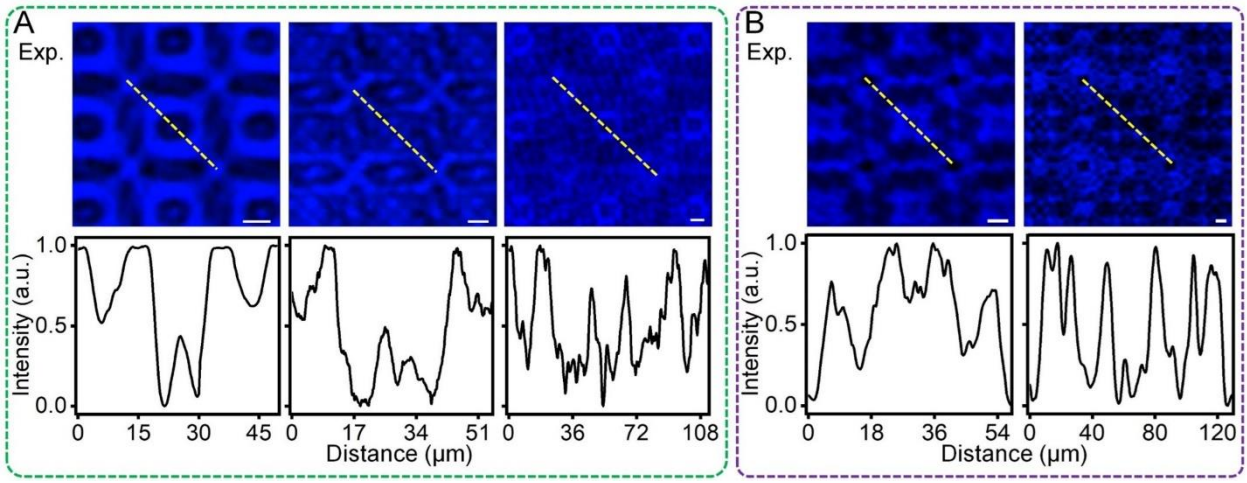

Supplementary Fig. 6.

Experimentally observed OM images of diffraction patterns and corresponding normalized intensity along the representative yellow dashed line. (**a**) The diffraction patterns have at least four gray levels when L = 9.81 or 19.98 μm, whereas only two-dimensional structure can be obtained since the weak interference intensity leads to the distortion in OM image when L exceeds 39.27 μm or reaches a sufficiently large value, where D is fixed at 20 μm and R = 0.289. (**b**) The complicated diffraction patterns with small patterns appear simultaneously when D and L both increase, where D = 20.11, L = 19.89 μm, and D = 40.23, L = 39.77 μm at R = 0.356. The experimental parameters are: H = 50 μm, U = 400 Vpp, and λ = 405 nm. Scale bar: 10 μm.

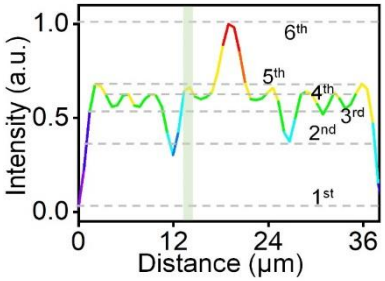

Supplementary Fig. 7.

Normalized intensity along the representative dashed line in Fig. 3B. The experimental parameters are: z = 1060 μm, D = 20.11 μm, L = 19.89 μm, H = 50 μm, U = 400 Vpp, and λ = 405 nm.

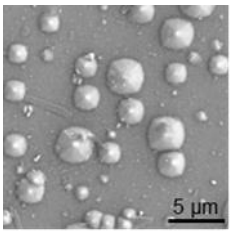

Supplementary Fig. 8.

Top view of SEM image of UPs-textured silicon wafer without trapping effects of microstructure.